One-dimensional flow of an ionized gas through a magnetic field

By R. M. PATRICK AND T. R. BROGAN
AVCO Research Laboratory, Everett, Massachusetts

(Received 11 July 1958)

As a primary step towards understanding the flow of a partially ionized gas in a magnetic field, we have studied both theoretically and experimentally the problem in which the gas flow is one-dimensional. This simplification permits a detailed calculation of the flow field and a quantitative comparison of the theory with observations made in a shock tube.

An ionized gas is composed of three species: electrons, ions and neutral particles. To take complete account of all the phenomena occurring when the high-velocity gas interacts with the magnetic field, the motion of all three species must be considered. When this is done, it is found that the electrical conductivity of the gas is a tensor dependent on both the magnitude and geometry of the magnetic field. However, when the collision frequency for the electrons is greater than their cyclotron frequency in a magnetic field, the gas may be treated as a continuum with a scalar conductivity. For such gas states, all of the observed effects for two experimental geometries in which the gas current forms closed loops in the magnetic field can be explained with a simple theory. The interaction produces a flow completely analogous to pipe flow with friction and no heat transfer, where the wall friction force is replaced by the magnetic body force which can choke the flow if the body forces are larger than a certain minimum value.

Using the same experimental geometries, the gas state is then adjusted so that the electrical conductivity is a tensor. Outstanding among the observed effects are ion slip, where the ions and neutrals travel through the field at different velocities, and Hall currents, generated by the drift of the charged particles across magnetic field lines. The observed effects again agree with the predicted values.

Introduction

This paper reports the results of a study of the one-dimensional flow of partially ionized argon through a magnetic field. The ionized argon is produced using the shock-tube technique described by Resler, Lin & Kantrowitz (1952). Argon was, chosen as a working fluid for two reasons. First, its properties at high temperature have been studied extensively in work by Resler *et al.* (1952), Lin, Resler & Kantrowitz (1955), Petschek, Rose, Glick, Kane & Kantrowitz (1955) and Petschek & Byron (1957). Second, the electrical conductivity which can be produced by strong shock waves in a shock tube is large (up to 10^4 mho/m) in comparison with other gases. This latter property permits appreciable inter-

actions between the moving gas and a magnetic field in dimensions appropriate to a shock-tube experiment.

In the experiments reported here, the gas has a component of velocity perpendicular to an externally applied magnetic field. This motion induces an electromotive force which in turn generates currents in the gas. The magnetic fields due to these induced currents are small compared to the applied fields, i.e. the magnetic Reynolds number R_m is much less than unity. Here, $R_m = \mu_0 \sigma v l$, where σ is the electrical conductivity of the gas, v the gas velocity perpendicular to the field, μ_0 the permittivity of free space and l the characteristic length of the interaction.

The energy transfer between the moving gas and the surroundings is negligible for these experiments. This implies that the gas currents form closed loops, with no part of their circuit external to the gas. The experimental geometries will be arranged so that the gas currents flow in a nearly uniform magnetic field and the current density j in the gas is given by $j = \sigma v B$, where B is the strength of the applied magnetic field.

If the Mach number M_1 of a shock wave and the initial pressure p_1 of the gas through which it is propagating are known, all the gas properties behind the shock are determined. Throughout this paper, these two parameters will be used to specify the gas conditions at the entrance to the magnetic field.

The experiments were carried out in two shock-tube geometries which will be called respectively the annular experiment and the end experiment. In the annular experiment, the channel area is constant. For the end experiment the channel area varies linearly in the flow direction, but the magnetic field is more uniform than in the annular experiment, and steady flow persists for a longer time. Also, the end experiment covers a larger range of variation of the experimental parameters than the annular experiment.

The electrical conductivity of a gas is influenced by a magnetic field. The conductivity at low field strength is a scalar quantity. For argon, the limiting conductivity at zero magnetic field was measured by Lin *et al.* (1955). As the magnetic field strength is increased, the conductivity becomes a tensor dependent on both the magnitude and geometry of the applied field. These latter effects have been considered by Schluter (1950, 1951). A measure of the extent to which the magnetic field influences the gas conductivity is given by the magnitude of the parameter $\omega_e \tau_e$, where ω_e is the cyclotron frequency of an electron in a magnetic field with strength B, and τ_e is the average time between collisions for an electron. As $\omega_e \tau_e$ approaches unity, the magnetic field begins to affect the gas conductivity in a significant manner.

For all of the conditions with which this paper is concerned, the flow Mach number of the gas entering the field exceeds unity. Therefore, the most important force exerted by the gas is its dynamic pressure $\frac{1}{2}\rho v^2$, where ρ is the gas density. To influence the motion of the gas in an important way, the force due to the interaction of the gas with the magnetic field must be of the order of the dynamic pressure. The precise conditions needed to produce such a situation are discussed in §II of this paper. To obtain a good estimate of the effects to be expected, we note that the gas current $j = \sigma v B$ interacting with the applied field B produces

a body force $F = \sigma v B^2$. If now the interaction extends over a length l, the pressure difference across the interaction region is $\Delta p = Fl = \sigma v B^2 l$. The extent to which the interaction has disturbed the flow is given by the ratio $\Delta p / \frac{1}{2}\rho v^2$. For an appreciable interaction, we have

$$\frac{\sigma B^2 l}{\rho v} \doteqdot \frac{1}{2}.$$

When the above condition is satisfied in the experiments, the supersonic flow entering the magnetic field is decelerated enough to cause choking and the formation of standing shock waves in the magnetic field.

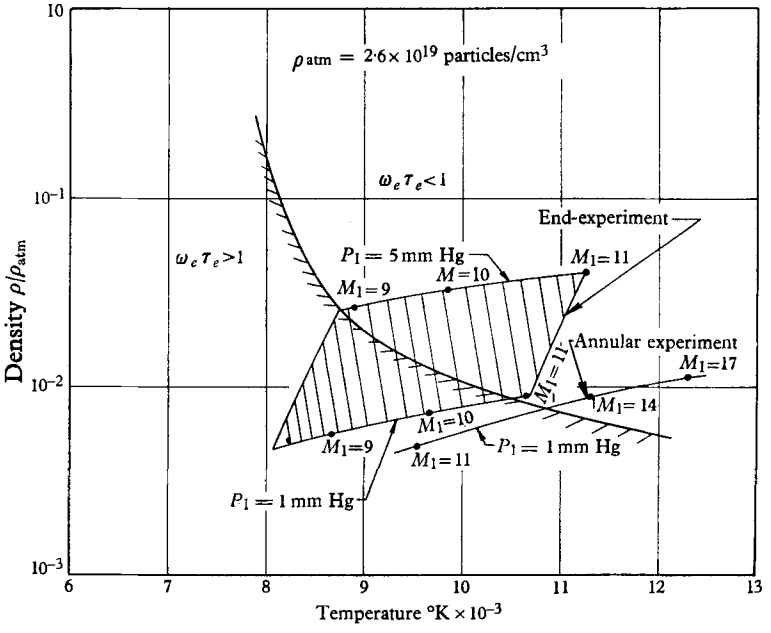

FIGURE 1. The density in atmospheres *vs* the temperature obtained in the experiments at the upstream end of the magnetic field.

Figure 1 shows the gas conditions at the upstream end of the magnetic field for both the experiments to be described in the next section. In the annular experiment, the initial pressure p_1 was held constant at 1 mm of mercury, so that the single line at the lower right corner of the figure gives the initial conditions for this experiment. Several different initial pressures were used for the end experiment. The resulting conditions are represented by the shaded area. On the line running from top left to lower right corners, $\omega_e\tau_e = 1$; the magnetic field B used to calculate ω_e is such that the interaction pressure equals the dynamic pressure of the moving gas with $l = 1$ cm. To the left of this line, the electrical conductivity of the gas is affected to a large extent by the magnetic field; to the right, it is largely unaffected.

In the next section, the experiments, technique and measurements are described. The final section is a development of the theory necessary to explain the experimental results.

I. Description of experiments

1. Annular experiment

The first of two experiments designed to study the flow of an ionized gas in a magnetic field is designated as the annular experiment. An overall sketch of the experimental arrangement is shown in figure 2. The shock tube is divided into two parts; that part to the left of the diaphragm contains argon at room temperature and at a pressure p_1 of 1 mm; that part to the right of the diaphragm (the driver) is filled with a combustible mixture at high pressure. When the mixture is burned, the pressure rises in the driver breaking the diaphragm and sending a strong shock wave to the left through the low-pressure argon. The gas behind this shock is heated, compressed and ionized.

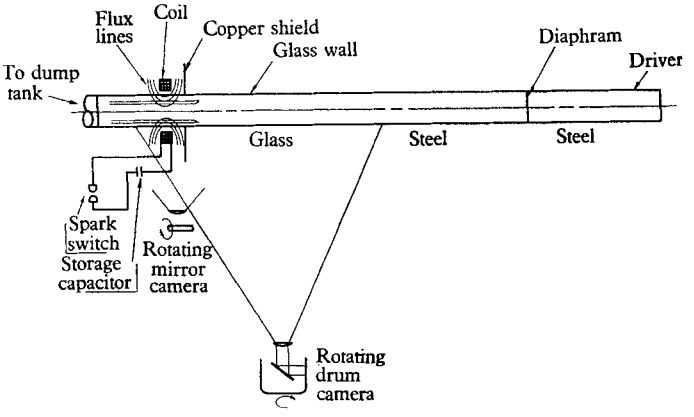

FIGURE 2. Schematic drawing of the shock-magnetic-field experiment.

After propagating through a 10 ft. section of steel tubing 1·5 in. in diameter, the shock enters a Pyrex tube of the same diameter. A slit is placed along the axis of this Pyrex tube, the slit being imaged in a high-speed, air-driven, rotating drum camera. The light emitted by the gas behind the shock is recorded on the film. A sample drum-camera photograph is shown in figure 3 (plate 1). The distance along the tube is the abscissa, while time is the ordinate. The horizontal lines are still pictures of the slit; the illuminated region is the image of the shock traversing the tube. The combination of the camera speed, plus the necessary geometrical factors, permits a precise determination of the shock speed and hence of all the gas properties behind the shock.

After passing through some 4 ft. of Pyrex tube, the shock finally arrives at the test region. Here, a cylindrical non-conducting tube of $1\frac{1}{8}$ in. outside diameter has been placed inside the $1\frac{1}{2}$ in. diameter Pyrex tube, forming an annulus $\frac{3}{16}$ in. thick between the two tubes (figure 4). The upstream edge of the inner tube is machined so that the shock wave enters the annular region without disturbance. The gas inside the inner tube is discarded.

A coil and a copper shield of $\frac{1}{4}$ in. thickness are placed around the annulus (figure 2). The separation between the coil and shield is $\frac{1}{2}$ in. The coil is connected to a 200 μF condenser through an air-spark switch timed to close (by a signal

from a photomultiplier upstream from the annulus) so that the current in the coil is a maximum when the shock reaches the shield. Since the coil, shield and condenser have a resonant frequency of only 1200 c/s, the magnetic field produced by the condenser discharge may be considered to be steady over a test time of some 20 μs.

The copper shield is several skin depths thick at the discharge frequency, so that no magnetic field penetrates through it. The radial component of the magnetic field in the annular region between the coil and shield is thus increased to about double the value it would have without the shield, while the axial field is reduced. The measured radial strength of the magnetic field varies about 20 % over the region of the annulus between the coil and shield. This non-uniformity, plus the presence of an axial field, can be important under some conditions which will be discussed shortly. Magnetic fields with a radial component as large as 6000 G are produced in the annulus between the coil and shield.

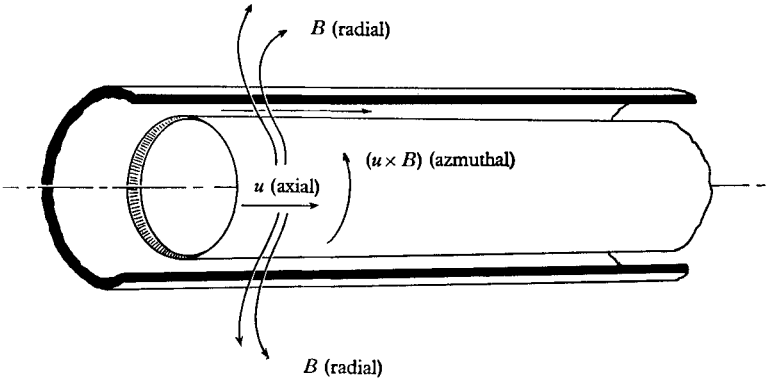

FIGURE 4. Schematic drawing of annular experiment showing co-ordinate system with direction of velocity, applied magnetic field and induced electric field.

As the gas behind the shock enters the magnetic field, the interaction of the gas velocity u with the radial magnetic field B induces an electric current of magnitude uB around the annulus (figure 4), causing a current to flow in the conducting gas. The current density j is equal to σuB, where σ is the gas conductivity. Note that no part of the current path is external to the gas, and that the current loops close in a constant magnetic field. The current j flowing across the magnetic field produces a body force of magnitude σuB^2 in a direction opposite to the gas velocity.

If the argon pressure before passage of the shock is 1 mm of mercury, the ionized gas behind the shock flows through the interaction region for about 20 μs. The time required for a sound wave in the hot gas to traverse the interaction region is about 3 μs, much less than the flow time. Due to this difference between flow time and time for a sound wave to traverse the interaction zone, it is reasonable to assume that steady flow is established through the magnetic field.

We have described previously how a high-speed drum camera is used to determine the shock velocity. A high-speed rotating mirror camera used in the same way produces an enlarged (x, t)-diagram for the gas in the vicinity of the inter-

action zone. Such a photograph for a typical run is shown in figure 5 (plate 2), along with an explanatory diagram. Again, the abscissa is the distance along the shock tube, while the ordinate is time. The hot gas behind the moving shock has an actual flow Mach number of about 2. It enters the interaction zone between the shield and coil from the left. The shock velocity is again given by the slope of the lower boundary of the illuminated region in figure 5. The body force, $\sigma u B^2$, causes the gas to decelerate in the interaction zone. A supersonic flow cannot be continuously decelerated through Mach number 1. Thus, if the magnetic field is sufficiently strong a shock wave will form in the interaction zone as shown in figure 5.

Because of the deceleration in the magnetic field, the shock propagating downstream from the interaction zone will travel at a lower velocity than the initial shock. As a measure of the degree of interaction with the magnetic field the difference in stagnation pressures, $p_{0_1} - p_{0_2}$, behind the initial and transmitted shocks may be compared to the computed pressure loss through the interaction zone. The change in stagnation pressure can be determined directly from the difference between the initial and transmitted shock velocities. The calculation is carried out in §II of this paper. Unfortunately, due to the small aperture of the rotating mirror camera used in this experiment, a visual record of the interaction could be obtained for only a small range of conditions of the gas behind the initial shock ($16 < M_1 < 18$). However, for this small range it was found that the loss in stagnation pressure across the magnetic field, as determined from the rotating mirror camera photographs, agreed with the predicted loss to within 30 %, as will be described in §II.

To study how the strength and geometry of the magnetic field influence the gas conductivity, the current in the gas was measured by a pick-up coil placed around the Pyrex tube forming the annulus. This coil was calibrated by measuring the pick-up due to a known high-frequency electric current in the interaction zone. This calibration current is produced by placing a coil in the interaction zone and exciting it with a signal generator. The gas current was measured over a large range of initial shock Mach numbers at a pressure of 1 mm. It was found that the electrical conductivity of the gas is drastically affected by the magnetic field (but not for those initial conditions for which rotating mirror photography was possible). These measurements will be discussed further in §2.

2. End experiment

The annular experiment suffers from three disadvantages: first, the non-uniformity of the magnetic field and its strong component in the flow direction; secondly, the relatively short testing time; and thirdly, the limited range of variation of the experimental parameters. These disadvantages offset the inherent simplicity of a constant area flow. Therefore, a second experiment which eliminates these difficulties has been performed.

For the end experiment, a diagram of which is shown in figure 6, the argon shock wave is reflected from the end of the $1\frac{1}{2}$ in. diameter shock tube. Gas from Region 3 (see figure 6) then flows radially outward through the end section; the channel area increases proportional to the radius. Since the gas pressure behind

the reflected shock is several hundred times the pressure before the arrival of the shock, the point indicated by * on figure 6 is a sonic point, as it is the point of minimum channel area. Beyond this point, the flow with no magnetic field is supersonic and the Mach number increases as we go outwards from the tube axis. The gas properties in the stagnation chamber, Region 3, are not affected by the flow beyond the sonic point, so that the radial mass flow is constant regardless of any gas-magnetic field interaction. This flow remains steady for times as long as 100 μs. The radial shock wave which precedes the gas flow eventually reflects back in towards the tube axis, but arrives in the test region too late to be of any consequence.

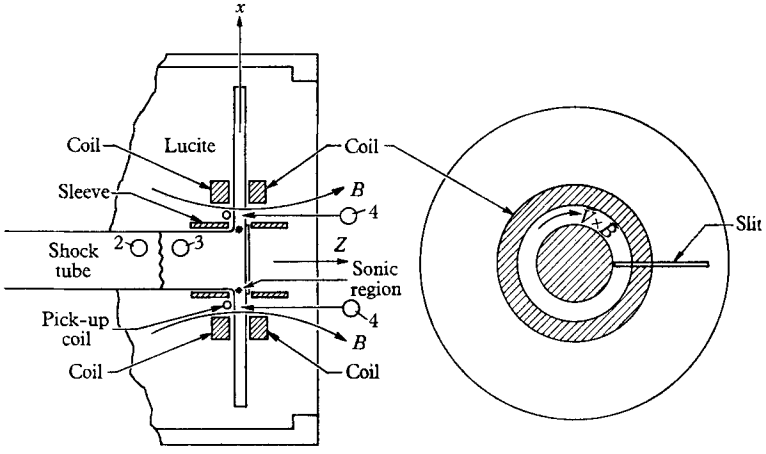

FIGURE 6. Schematic drawing of end experiment showing a side cross-section and end view.

The flow properties at the entrance of the magnetic field, Region 4, are determined by computing the properties of the gas in Regions 2 and 3, following the method outlined by Resler (1952), and matching the flow through the minimum area denoted by * on figure 6. The condition for this match is the continuity equation $\rho_3 u_3 A_3 = \rho^* u^* A^*$, where A^* is the channel area at the sonic point.

The flow conditions in Region 4 without an applied magnetic field were computed by using the conventional methods of one-dimensional isentropic channel flow. These flow calculations were checked by measuring the light emitted from the radial slit (figure 6). In these experiments argon was used as the working gas. The light emitted by highly ionized argon is due mainly to an electron-ion recombination continuum described by Petschek *et al.* (1955). Its intensity distribution in the visible region is given by

$$I_{(\nu)} = K \frac{N_e^2}{T^{\frac{1}{2}}},$$

where K is a constant, ν the frequency, N_e the number density of electrons, T the temperature and $I_{(\nu)}$ is the radiation per cubic centimetre per unit frequency interval. The measured light intensities check the one-dimensional flow calculations within the experimental error of the light intensity measurements (20 %).

When the magnetic field is present in Region 4 (figure 6), the gas flows radially outward through the field produced by the two coils and copper shields. The coil is connected to a 200 μF condenser through an air spark switch which is timed to close so that the current in the coils is a maximum during the experiment. The discharge frequency is 1·1 kc/s, the copper shields are several skin depths thick at this frequency, so that little magnetic field penetrates through the shields. In figure 7, the z-component of the magnetic field is plotted *vs* distance from the shock-tube axis. The radial component of the field is never greater than 4 % of the maximum axial field. The difference between this geometry and that of the annular experiment, where there is a strong field component in the flow direction, is important when the effect of magnetic field on gas conductivity is considered.

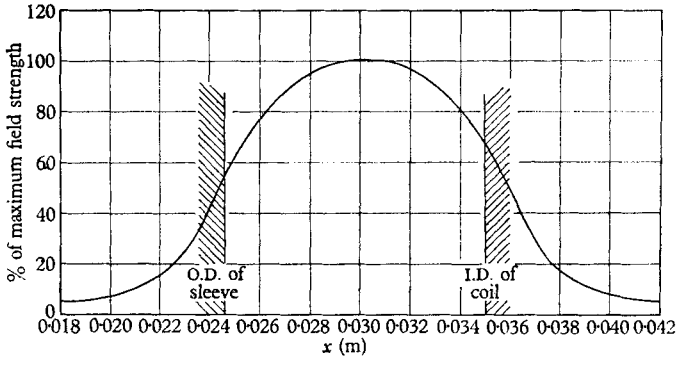

FIGURE 7. The magnetic field distribution in Region 4 as a function of radial distance.

The radial gas velocity v crossing the magnetic field B induces an electric field as shown in figure 6. This field closes in the gas, causing a current of magnitude σuB, and a body force directed towards the axis of the tube. The effect is to decelerate the gas, but this effect is competing with the increasing channel area which tends to accelerate the gas. For strong fields, the gas is decelerated, again producing shock waves in the interaction zone between the coils and shields.

A slit is installed radially outward from the tube axis as shown in figure 6, and the rotating mirror camera is again used to study the interaction of the gas flow with the magnetic field. A typical mirror-camera photograph, along with an explanatory diagram, is shown in figure 8 (plate 3). The exposed region on the left is the interaction zone. The distinct vertical line dividing two regions of different light intensity in this interaction zone is a shock wave produced by the interaction between the flow and field. The radial position of the shock changes during the test time, since the magnetic field varies slightly in a period of 100 μs. However, the field variation is so slow that the flow may be assumed to be steady at any given time. The dark region is the location of the coil. The shock reflecting radially is shown on the right. It is seen that this shock never reaches the interaction zone. Figure 9 (plate 3) is a mirror-camera photograph for the case of a very strong field; in this case, the shock wave is actually reflected by the magnetic field. Steady flow is not possible at these large field strengths.

Due to the high gas density and strong magnetic field obtainable with the end experiment, the gas-field interaction could be studied with the mirror camera over a large range of initial gas conditions (see figure 1). The photographic study could be extended to the region where the gas conductivity is affected by the magnetic field.

The electric current in the gas is measured by a pick-up coil in a manner identical to that in the annular experiment. These gas-current measurements are discussed in §II.

Figure 10 (plate 4) is a photograph of the apparatus for the end experiment. The shock tube is the long pipe entering the picture from the right. The radial flow is established in the large end cap on the tube; this cap also contains the coils and shields. The high-speed, air-driven, rotating-mirror camera is on the extreme right. It has a maximum aperture of f3·5, and a maximum writing speed of 0·5 cm/μs. Various photomultipliers and optical equipment used in the study of the gas properties are also shown.

In the following section, the experimental observations will be compared with a simple theory of one-dimensional gas flow in a magnetic field.

II. Theoretical description of the experimental results

1. Mach-number variation

The equation for the Mach number M_1 as a function of the ratio of heat capacities γ, channel area A, and body forces X is given by Shapiro & Hawthorne (1947) for steady, one-dimensional flow without friction or heat transfer

$$\frac{dM^2}{M^2} = -\frac{2\{1+\frac{1}{2}(\gamma-1)M^2\}}{1-M^2}\frac{dA}{A} + \frac{2\gamma M^2\{1+\frac{1}{2}(\gamma-1)M^2\}dX}{(1-M^2)\rho v^2}, \tag{1}$$

where v is the magnitude of the gas velocity $\mathbf{v}$ and ρ is the gas density. Equation (1) applies to both experimental geometries described in the previous section where the current loops close in the gas. The electric current in the gas can be written

$$\mathbf{j} = \sigma(\mathbf{v}\times\mathbf{B}), \tag{2}$$

where $\mathbf{j}$ is the gas current-density vector, $\mathbf{B}$ the magnetic field and σ the effective gas conductivity.

In this analysis, displacement currents are neglected. Also, the net charge density is assumed to be zero, since at the gas densities used in the experiments the Debye shielding distance is small compared to both the mean free path and the appropriate gyro radius. We may regard equation (2) as defining an effective conductivity σ for currents in the $(\mathbf{v}\times\mathbf{B})$-direction. The effective conductivity depends not only on the temperature and density of the gas for all the experimental conditions, but in some cases depends also upon the magnetic field strength and field geometry.

The component of the magnetic field perpendicular to the gas velocity alone contributes to the current density. The body force per unit volume is $\mathbf{j}\times\mathbf{B}$, and its component X parallel to the flow direction is

$$X = \sigma v B_{\mathrm{perp}}^2,$$

where B_{perp} is the component of B perpendicular to the flow direction.

With the above definition of the effective gas conductivity, one may write the equation for the change in M (equation (1)) as follows:

$$\frac{dM^2}{M^2} = -\frac{2\{1+\frac{1}{2}(\gamma-1)M^2\}}{1-M^2}\left\{\frac{dA}{A} - \frac{\gamma M^2 \sigma B^2}{\rho v A}dx\right\}, \tag{3}$$

where x is the co-ordinate parallel to **v**.

Equation (3) expresses the change in M in terms of the channel area A, and the ratio of magnetohydrodynamic body force to gas momentum, $\sigma B^2 A\,dx/\rho v A$. The analysis will be divided into two parts. The first part deals with the annular experiment where there is no area change and hence $dA = 0$ in (3). The second part deals with the end experiment where the complete equation is integrated to describe the experimental results.

2. Constant area flow (annular experiment)

For the case of constant area, (3) simplifies to

$$dS = \frac{(1-M^2)\,dM^2}{2\gamma M^4\{1+\frac{1}{2}(\gamma-1)M^2\}}, \tag{4}$$

where S is a non-dimensional interaction variable defined by $S = \sigma B^2 x/\rho_0 v_0$ and $\rho_0 v_0$ is the mass flow per unit area. Equation (4) describes the variation of M with distance in the flow direction. M decreases with distance for supersonic flow and increases for subsonic flow. The effect of the interaction is to produce a situation completely analogous to pipe flow with friction and no heat transfer. The state of the gas is described by a Fanno line. If the 'pipe' is long enough, M at the exit will be unity, i.e. the flow chokes.

To find the value $S = S_0$ at which the flow chokes, we integrate (4) from $M = M_0$ to $M = 1$, and assume no shock waves between the limits of integration. The result is

$$S_0 = \frac{1}{2\gamma}\left[\left(\frac{\gamma+1}{2}\right)\log\left\{\frac{2}{\gamma+1}\left(\frac{1}{M_0^2}+\frac{\gamma-1}{2}\right)+\frac{M_0^2-1}{M_0^2}\right\}\right]. \tag{5}$$

Here S_0 is the minimum value of S which will choke the flow with an initial Mach number M_0 (σ is taken to be constant, an approximation accurate to within 20 % for the annular experiment). The function S_0 is plotted against M_0 on figure 11 for $\gamma = 1{\cdot}13$, which is representative of argon under the experimental conditions.

Using the values of electrical conductivity measured by Lin *et al.* (1955), the experimental arrangement gave $S_{\max} = 0{\cdot}5$ ($S_{\max}$ corresponds to $x = l$, the length of the interaction region). The conditions behind strong shock waves in argon are such that the Mach number at the entrance of the field region is approximately equal to 2 for the experimental conditions in the annular experiment (Resler *et al.* 1952). Since $S_{\max} = 0{\cdot}5$, and M upstream is equal to 2, $S_{\max}$ is greater than that value S_0 necessary to cause M at the exit of the field to be equal to unity (figure 11). Therefore, a shock forms in the interaction region which makes the flow subsonic downstream from it. The flow then accelerates to $M = 1$ at the exit of the field. The variation of M in the field region is shown in figure 12.

Furthermore, it is evident by continuity that the gas properties at the exit of the field are independent of the shock position in the field for $S_{max} \geqslant S_0$, and less than that value of S_{max} which causes a standing shock at the entrance of the field.

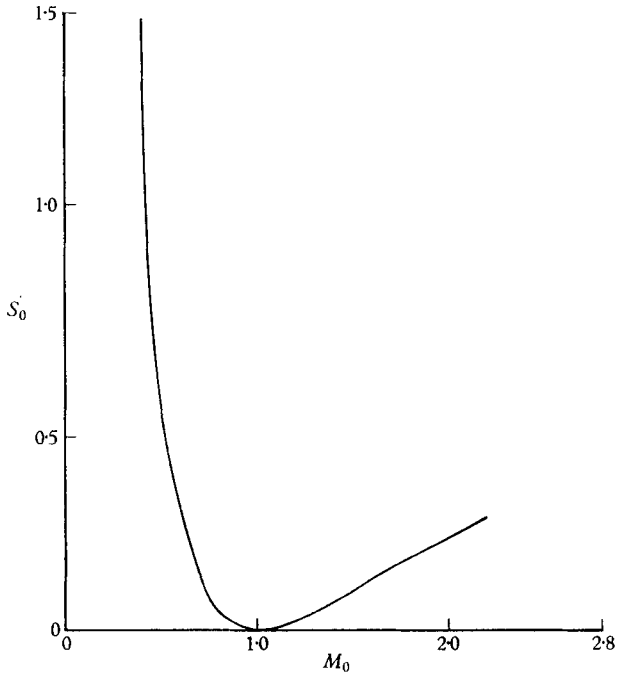

FIGURE 11. Interaction length necessary to change the Mach number M to unity, expressed as a function of the Mach number.

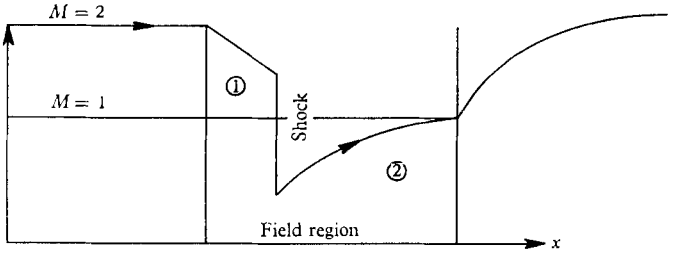

FIGURE 12. Change in Mach number in the field region as a function of distance in the stream direction.

The loss in stagnation pressure p_0 for $S_{max} \geqslant S_0$ is easily computed using the relationships given by Shapiro & Hawthorne (1947):

$$\frac{dp_0}{p_0} = -\frac{\gamma M^2}{\rho_0 v_0 v} dX = -\gamma M^2 dS. \tag{6}$$

Substituting for dS from (4), we have

$$d(\log p_0) = \frac{(M^2-1)}{M^2\{2+(\gamma-1)M^2\}} dM^2. \tag{7}$$

Since the shock position does not influence the exit conditions, we integrate equation (7) between $M = M_0$ and $M = 1$ to obtain

$$\frac{p_{0_1}}{p_{0_2}} = \frac{1}{M_0}\left[\left(\frac{2}{\gamma+1}\right)\left(1+\frac{\gamma-1}{2}M_0^2\right)\right]^{\frac{1}{2}(\gamma+1)/(\gamma-1)}. \tag{8}$$

The exit conditions, Region 2 of figure 5 (plate 2), are now completely determined.

The gas pressure and velocity must match across the entropy line dividing the gas which has passed through the field, Region 3 in figure 5 (plate 2), from the gas behind the transmitted shock Region 4. Using the theoretical exit properties as initial values for an unsteady expansion downstream of the field region, the gas properties behind the transmitted shock were computed. The match is carried out far enough downstream so that the expansion is essentially complete. The predicted velocity of the transmitted shock was compared to the experimental value measured on the mirror camera photographs described in §I (see figure 5). It was possible over the small range of the experiments to predict the difference between the initial and transmitted shock velocities to within 15 %: in other words, the change in stagnation pressure across the interaction could be predicted to within 30 %.

3. Channel flow with varying area (end experiment)

The particular case of steady, one-dimensional flow considered here is that case where the cross-sectional area A is directly proportional to the co-ordinate x in the flow direction. For this case, equation (3) becomes

$$\frac{dM^2}{M^2} = -\frac{2\{1+\frac{1}{2}(\gamma-1)\}M^2)}{1-M^2}\frac{dx}{x} + \frac{2\gamma M^2\{1+\frac{1}{2}(\gamma-1)\,M^2\}}{1-M^2}\left[\frac{2\pi\sigma B^2 x}{\rho v A}\right]dx. \tag{9}$$

The flow properties in the magnetic field, Region 4 of figure 6, were computed using this equation. Up to the entrance of Region 4, the flow properties were determined by using only the first term on the right-hand side of (9).

Solutions of (9) were obtained using initial conditions corresponding to several values of M_1 and p_1. A particular set of solutions for $M_1 = 10$ and $p_1 = 5\,\text{mm}$ are presented in figure 13 for various values of the maximum magnetic field strength. The values of $B/B_{\max}$ as a function of x are taken from figure 7. Values of σ were computed for conditions at the entrance to Region 4, i.e. $M = 1{\cdot}1$. Then, in Region 4, σ was taken to be proportional to $T^{\frac{3}{2}}$, where T is the gas temperature (Lin *et al.* 1955). Values of γ were computed from the thermodynamic functions for argon, and these values were then used in the numerical solution of (9). For the calculations, it is assumed that the gas is always in thermodynamic equilibrium.

The upper curves of figure 13 are straightforward solutions of (9) in the supersonic regime. The same initial conditions were used for each value of B, since the first term on the right-hand side of (9) is large compared to the second term at the upstream end of the field region. The lower curves (subsonic regime) were computed by integrating from large values of x to small values, using an initial $M = 0{\cdot}99$. The initial point was determined by computing dM^2/dx from (9) and finding the largest value of x where this quantity is positive. For a given $B_{\max}$,

this point was taken to be the value of x beyond which the magnetic field would not affect the flow, since the magnitude of $B^2(x)$ decreases rapidly with increasing x (figure 7). The vertical lines on figure 13 represent shock waves in the flow obtained by matching the supersonic and subsonic curves for each value of B_{max}.

The physical argument for this procedure is as follows. At the entrance of the field region M is greater than unity (figure 13). Entering the field, the value of M at first increases due to the increasing area. The value of M decreases when the second term on the right-hand side of equation (9) dominates, i.e. the magnetic body forces have a greater effect than the area change. For the conditions of figure

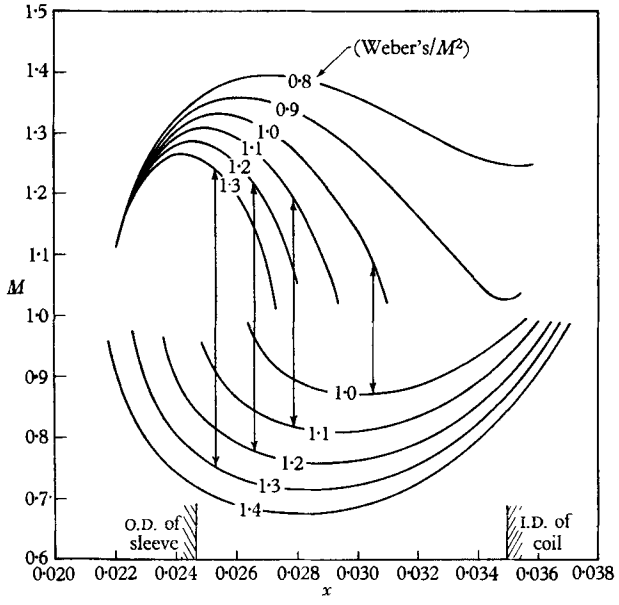

FIGURE 13. The solutions of equation (5) in Region 4, showing the shock waves connecting the supersonic and subsonic regimes.

13, a maximum field strength of 9000 G causes the value of M to decrease almost to unity at the exit of the field. Beyond the field region, M increases. For higher values of B, M decreases more rapidly in the supersonic regime, but cannot decrease continuously through unity as this would correspond to a decrease in entropy. Since the flow downstream from the field region is supersonic, and since the area increases continuously, the minimum value of M at the exit of the field is unity. When the second term in (9) is large ($B_{max} > 9000$ G), this corresponds to M increasing towards unity from a subsonic value in the field. Hence, for sufficiently high values of B_{max}, the flow at the exit of the field will always be such that M is equal to unity if the flow downstream is supersonic. For still larger values of B_{max}, no shock matching condition can be made between the subsonic and supersonic curves in Region 4. An unsteady shock will then be produced which propagates upstream. An example of this situation was shown in figure 9 (plate 3). The flow behind this unsteady shock expands smoothly so as to lead to Mach number unity at the exit of the field.

The shock location was measured from several mirror-camera pictures for experimental conditions that correspond to the theoretical results given in figure 13. These experimental results are plotted in figure 14 along with the computed shock location as a function of $B_{\max}$. For the field strengths involved (of the order of 10^4 G) the electrons in the ionized gas do not make a complete gyro orbit between collisions. The theory using a scalar conductivity, which is

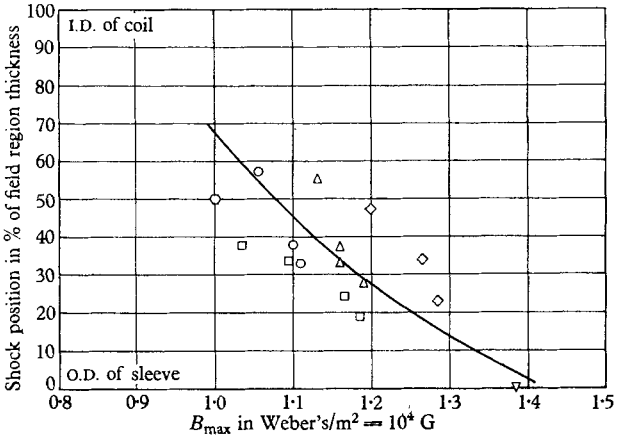

FIGURE 14. The theoretical and experimentally determined shock locations for $M_i = 10$, $p_1 = 5$ mm in the shock tube for various field strengths in Region 4. —, theoretical shock position for $M_i = 10$; $p_i = 5/760$ atm. *Note.* Each type of symbol corresponds to one mirror-camera picture.

a function only of the state of the gas, agrees with the experimental results. Data was taken over the range $9 \leqslant M_1 \leqslant 11$ and $2 \leqslant p_1 \leqslant 10$ mm. These results also agree with the theoretical predictions with errors of the same order as in figure 14.

For conditions with $p_1 < 2$ mm and $M_1 < 11$ (figure 1), the field strengths necessary to cause a shock to form in the field are such that the electrons make a complete gyro orbit between collisions.

4. Non-Scalar Conductivity ($\omega_e \tau_e > 1$)

In the presence of a magnetic field, there are two conditions that cause the effective conductivity σ in equation (2) to be less than the scalar value (Schluter 1950, 1951). The first condition is that the electrons can make a complete gyro orbit between collisions, that is $\omega_e \tau_e > 1$. This gives rise to an electromotive force (the Hall potential) in the $(\mathbf{j} \times \mathbf{B})$-direction which, if a path is provided, may cause an electric current (the Hall current) to flow in this direction. If the conditions are such that the Hall current can flow unimpeded, the conductivity is reduced as follows:

$$\sigma = \frac{\sigma_0}{1 + (\omega_e \tau_e)^2}, \tag{10}$$

where σ_0 is the conductivity in the absence of a magnetic field.

The second condition is the effect of the relative difference between the ion velocity with respect to the magnetic field and the velocity of the neutral particles with respect to that field. This gives rise to a decreased conductivity

$$\sigma = \frac{\sigma_0}{1+\omega_e\tau_e\omega_I\tau_I}, \tag{11}$$

where ω_I is the appropriate cyclotron frequency for ions, and τ_I is the mean free time for ion-neutral collisions. The above expression assumes that the Hall current is zero. A brief discussion of these two effects is given in the Appendix.

If the magnetic field has a large component along the flow direction, as in the annular experiment, one would expect to find that equation (10) describes the gas conductivity since the electrons will tend to flow along field lines. If, as in the end experiment, the component of the field in the flow direction is small, one would expect that equation (11) would describe the behaviour of the conductivity.

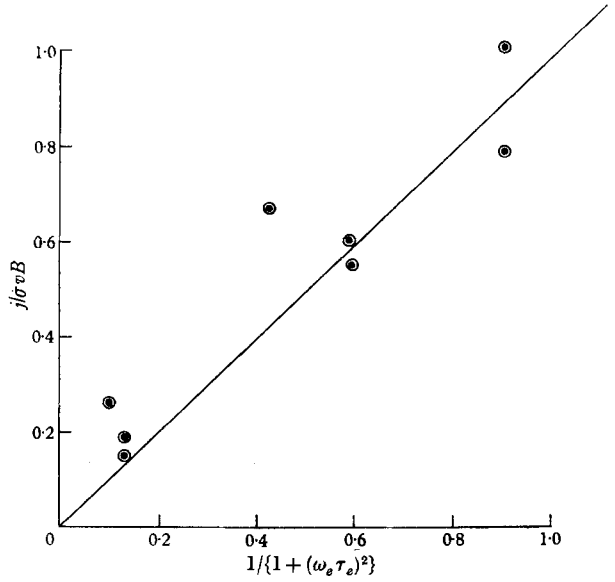

FIGURE 15. The current j measured in the annular geometry divided by σvB, the current if the effective conductivity is scalar, *vs* the factor, $1/\{1+(\omega_e\tau_e)^2\}$.

Annular experiment. The results of the gas-current measurements for the annular experiment are shown in figure 15. The ratios of the measured gas current density j to $\sigma_0 vB$ are plotted *vs* $1/\{1+(\omega_e\tau_e)^2\}$. The variation in $\omega_e\tau_e$ corresponds to a variation in M_1 at $p_1 = 1$ mm. The points are close to the theoretical value predicted by using equation (10) for the gas conductivity. The magnitude of the gas currents indicates that Hall currents can flow along field lines when these lines have an appreciable component parallel to the flow direction.

End experiment. A plot of the shock location as a function of M_1 is given in figure 16 for $p_1 = 1$ mm. The solid curve represents the theoretical shock locations found in the same manner as for figure 13 and with scalar conductivity proportional to $T^{\frac{3}{2}}$. The computed curve and the experiments are for $B_{\max} = 5000$ G.

The dashed curve represents the theoretical shock positions using (11) for σ, which takes ion slip into account. The measured shock locations (circles) indicate that ion slip becomes important under these conditions. The effect of the magnetic field on the gas conductivity was computed using an average for B and an average ion density. This use of average quantities may account for some of the discrepancies between the calculated and measured shock positions. Further, there is an uncertainty in the measured shock position at this low gas density which is equal to approximately 20 % of the field region length.

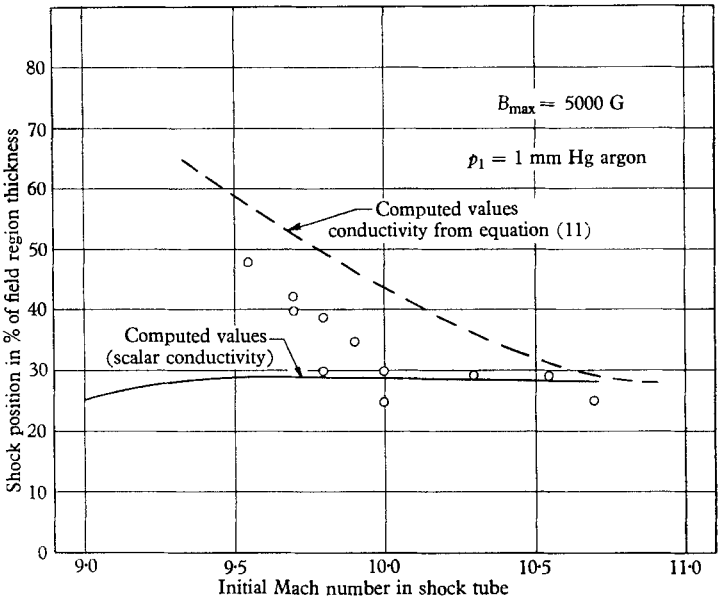

FIGURE 16. The theoretical and experimental shock locations in Region 4 for a constant magnetic field strength, showing one curve which was computed using a scalar conductivity and one which used equation (11) for the conductivity in equation (9).

For conditions such that $\omega_e \tau_e > 1$, the measured gas currents are plotted in figure 17. The three curves in this figure represent the total gas current computed by evaluating the integral

$$I = 2t \int \sigma v B \, dx \tag{12}$$

through the field region from shield to coil; $2t$ is the channel thickness. For $\sigma = \sigma_0$, the values of σ_0, v and B in the integral were obtained from the data used to compute the shock locations. The other two curves were obtained by using the value of σ given by (10) and (11). From the results plotted in figure 17, it appears that there is no current in the flow direction, i.e. no Hall current, when $M_1 > 9$ at $p = 1$ mm. The measured currents do agree with the values to be expected using (11) for σ. This indicates again that the predominant effect is ion slip, i.e. the difference in velocity between ions and neutral particles.

If no currents can flow in a direction perpendicular to $\mathbf{v} \times \mathbf{B}$, then a potential $\omega_e \tau_e (\mathbf{v}_I \times \mathbf{B})$ will exist in the flow direction, where $\mathbf{v}_I$ is the ion velocity. This was

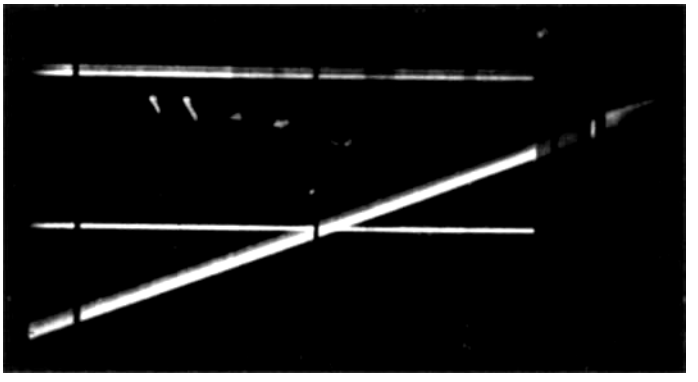

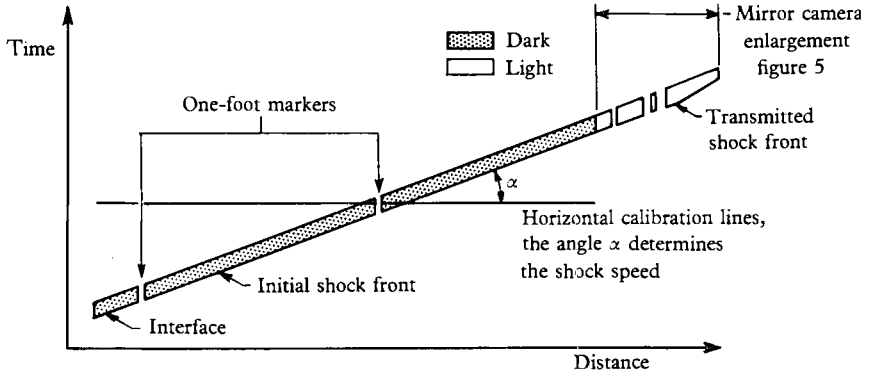

FIGURE 3 (plate 1). Drum-camera photograph showing a time (ordinate) *vs* distance (abscissa) picture of the shock phenomena over 3 ft. of the shock tube with the magnetic field on the right. The horizontal line is a still picture of the slit.

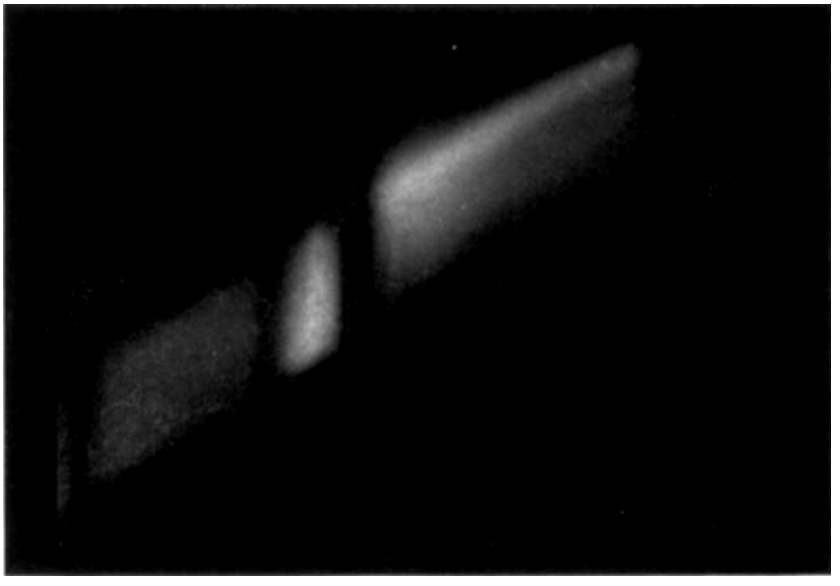

FIGURE 5 (plate 2). Mirror-camera photograph showing a time (ordinate) *vs* distance (abscissa) picture of the shock passing through the magnetic field.

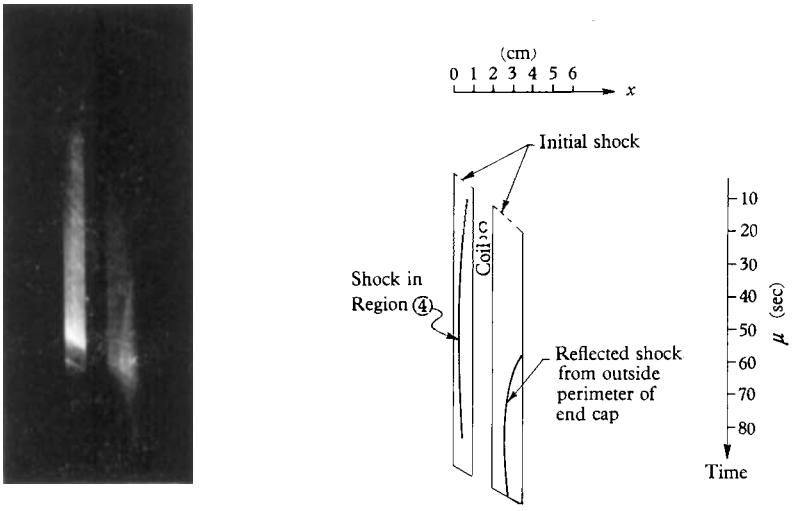

FIGURE 8 (plate 3). A mirror-camera photograph of the light emitted from the slit on the end cap, figure 9 (plate 4), showing the standing shock, and a schematic drawing of the photograph.

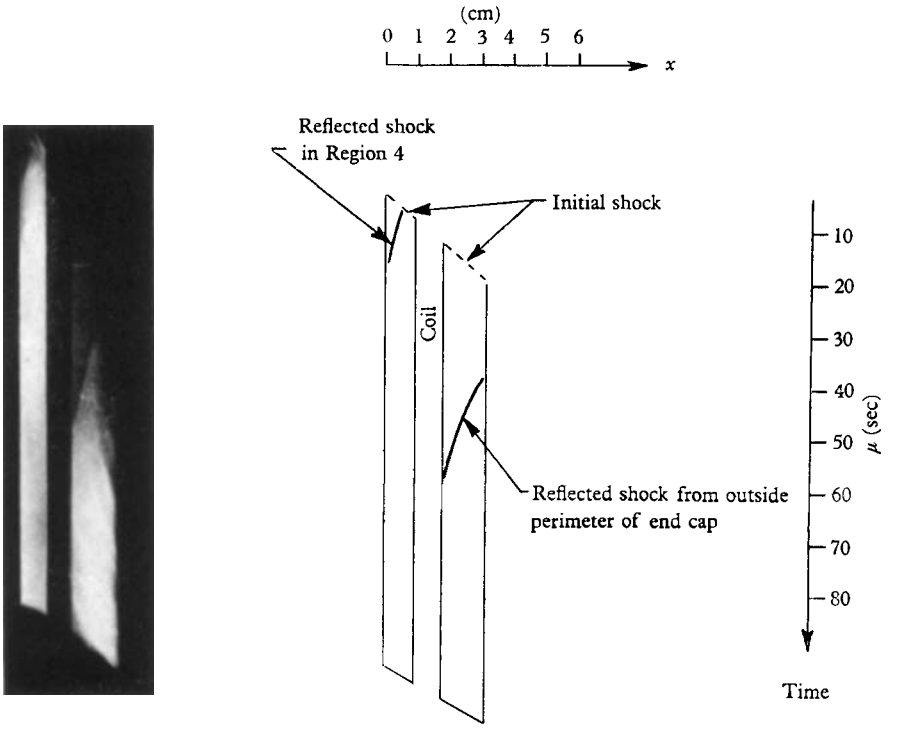

FIGURE 9 (plate 3). A mirror-camera photograph of the end-cap slit showing a reflected shock produced by a magnetic field in Region 4.

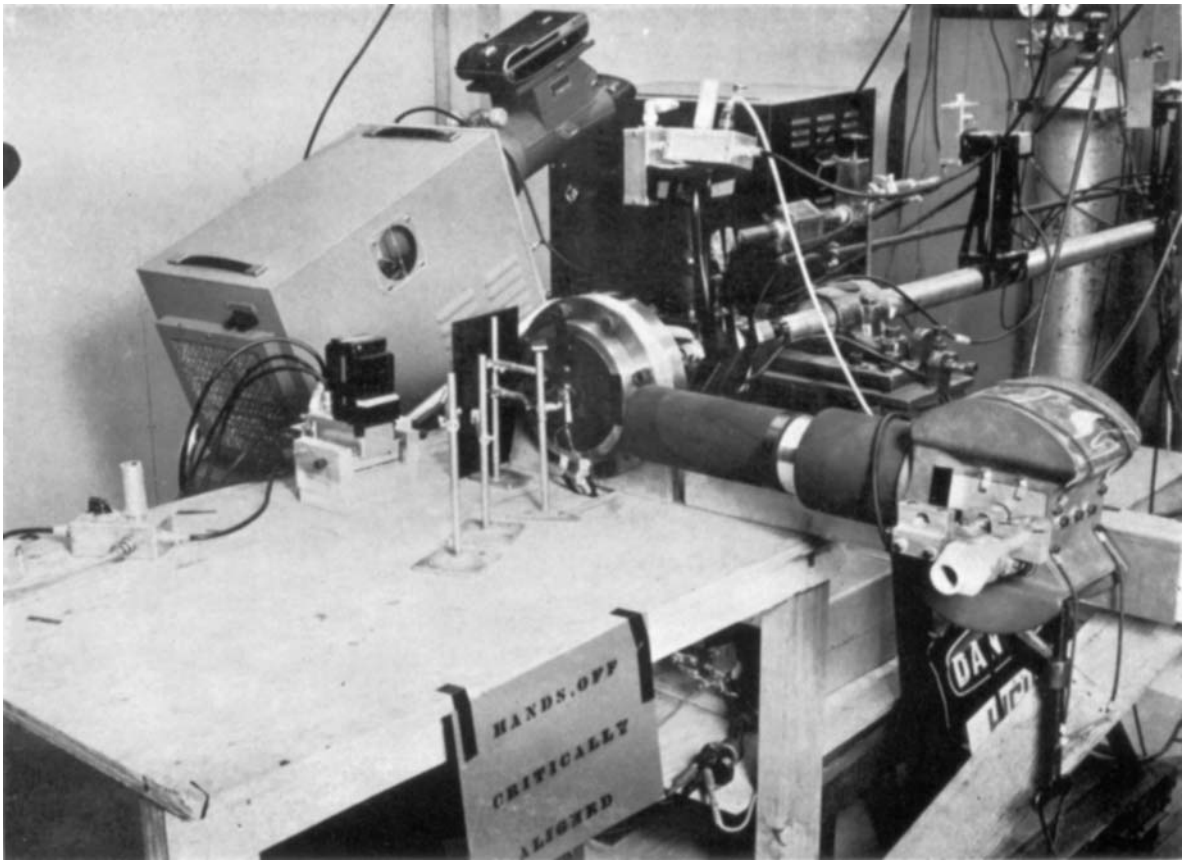

FIGURE 10 (plate 4). An overall photograph of the experimental arrangement, showing the shock tube, end experiment, photomultipliers, mirror camera, and some of the additional instruments.

shown by Schluter (1951). In order to estimate whether or not there could be a current in the flow direction capable of causing the effective conductivity to fall below the value given in equation (11), one must consider the possibility of current loops in the flow direction which close in the boundary layer. This effect

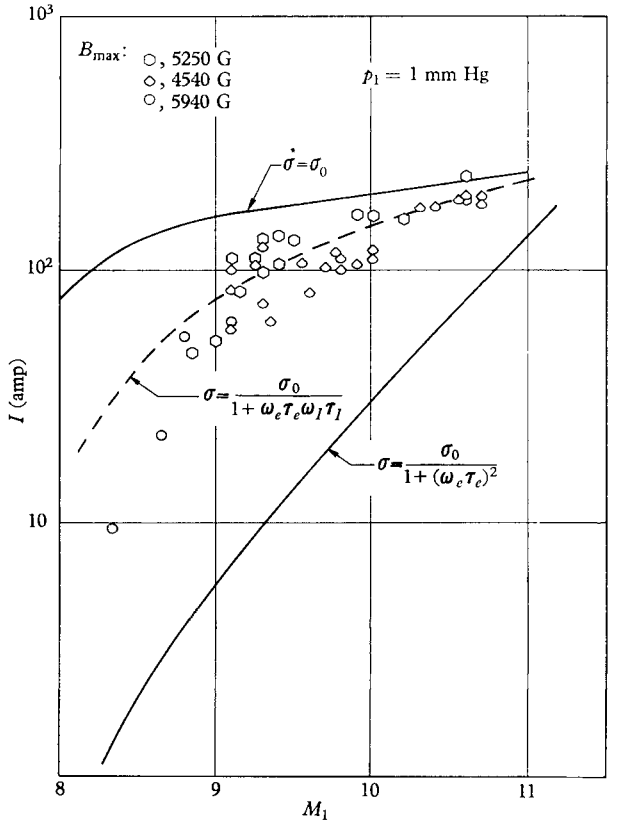

FIGURE 17. The solutions of equation (8) for various values of σ, the conductivity, together with measured values of the gas current I plotted as a function of the initial Mach number in the shock tube, M_i, for $p_1 = 1$ mm and for various values of B_{max}.

is estimated in the Appendix where we show that the current in the $(\mathbf{v}\times\mathbf{B})$-direction, J_y, is given by

$$J_y = \sigma_0 v_I B t\left\{\frac{1+\dfrac{\sigma_{0B}}{\sigma_0}\dfrac{\delta}{t}\left(\dfrac{1+w_e^2}{1+w_{eB}^2}\right)\dfrac{1}{1+w_e^2}}{1+\dfrac{\sigma_{0B}}{\sigma_0}\dfrac{\delta}{t}\left(\dfrac{1+w_e^2}{1+w_{eB}^2}\right)}\right\}, \tag{13}$$

where $2t$ is the thickness of the inviscid flow region, δ the thickness of the boundary layer, σ_{0B} the boundary-layer conductivity with no magnetic field, $w_e = \omega_e\tau_e$ for the inviscid region, and $w_{eB} = \omega_e\tau_e$ in the boundary layer.

If no effect due to electrons rotating about field lines is present,

$$I = 2t\int \sigma_0 v_I B\, dx.$$

The data on figure 17 indicate that there might be an important effect due to electrons rotating about field lines for values of M_1 below 9. When conditions at the entrance of the field region correspond to values of M_1 between 8 and 9, the maximum displacement thickness for the boundary layer in Region 4 of figure 6 is less than one-tenth the inviscid flow thickness. The maximum possible change in I for a given value of δ would occur if $\sigma_{0B} = \sigma_0$ and $w_{eB} = 0$. With the boundary-layer thickness encountered under the flow conditions of figure 17, this maximum change in I is less than 10 %. Therefore, we conclude that the presence of Hall currents closing in the boundary layer does not explain the low value of I for $M_1 < 9$.

In all of the calculations, we have tacitly assumed that the gas is in thermodynamic equilibrium. The time for the gas to reach equilibrium can be estimated using a method outlined by Petschek & Byron (1957). Applying this method to calculate the time for the gas to reach equilibrium behind the reflected shock, Region 3 of figure 6, we find that in the available test time the gas in Region 3 does not reach equilibrium for $M_1 < 9$. The lack of equilibrium with $M_1 < 9$ probably accounts for the discrepancy between the measured values of I and those predicted by using equation (11) for the conductivity.

Conclusions

From the results of experiments described in this report one may make the following conclusions.

1. One-dimensional iso-energetic, steady flow of a compressible fluid in a magnetic field with no heat transfer or friction may be described by a theory which takes into account the area change of the channel and the magnetic body forces.

2. The effect of a steady magnetic field on one-dimensional iso-energetic gas flow is similar to friction due to viscosity and with sufficient field strengths will produce choking.

3. The maximum effect of a magnetic field is to cause the Mach number at the exit of the field to be equal to unity.

4. In the presence of a magnetic field, the electrical conductivity of a gas is reduced. This reduction is due to (*a*) Hall currents, or (*b*) ion slip.

The authors wish to express their appreciation to A. R. Kantrowitz, H. E. Petschek, R. J. Rosa and Prof. Max Krook for their interest and helpful suggestions. They are also indebted to John Lothrup and Lawrence McInnis for their help in carrying out the experiments.

This work was sponsored by the Ballistic Missile Division, Air Research and Development Command, U.S. Air Force, under Contract AF 04(645)-18.

Appendix

For the experiments described in this paper, one may consider the following special gas conditions. The degree of ionization $\alpha = Ne/NN_A$ is small (approximately 10^{-2} for most experiments), and the electron density is very nearly equal to the ion density (cf. Lin *et al.* 1955). If one neglects terms involving the ratio of

the electron mass m_e to the atom and ion masses, the momentum equation for the electrons leads to the following expression for the current in the gas

$$\mathbf{j} = N_e e(\mathbf{v}_I - \mathbf{v}_e) = \sigma_0 \left\{ \frac{\operatorname{grad} p_e}{N_e e} + \mathbf{E} + \mathbf{v}_e \times \mathbf{B} \right\}, \tag{A 1}$$

where N_e is the number density of electrons, e is the charge on the electron, $\mathbf{v}_I$ is the ion velocity, $\mathbf{v}_e$ is the electron velocity, σ_0 is the gas conductivity in the absence of a magnetic field, p_e is the electron pressure and $\mathbf{E}$ is the electric field. In our experiments, $\mathbf{E} . (\mathbf{v}_I \times \mathbf{B}) = 0$.

The following results, due to Schluter (1950, 1951), give the components j_{par} and j_{perp} of the gas currents, respectively, parallel to and perpendicular to the $(\mathbf{v}_I \times \mathbf{B})$-direction:

$$j_{\text{par}} = \frac{\sigma_0 v_I B}{1 + (\omega_e \tau_e)^2} = \sigma_{\text{par}} v_I B, \tag{A 2}$$

$$j_{\text{perp}} = \frac{\sigma_0 v_I B \omega_e \tau_e}{1 + (\omega_e \tau_e)^2} = \sigma_{\text{perp}} v_I B, \tag{A 3}$$

where

$$\omega_e \tau_e = \frac{B e}{m_e} \frac{m_e}{N_e e^2} \sigma_0.$$

The σ defined in equation (10) is just the σ_{par} of equation (A 2), and gives the effective conductivity in $(\mathbf{v}_I \times \mathbf{B})$-direction if currents are allowed to flow in the stream direction with no external impedance.

For the end geometry experiments described in this paper currents perpendicular to the $(\mathbf{v}_I \times \mathbf{B})$-direction in Region 4 can close only in the boundary layer. If no currents can flow in a direction perpendicular to $\mathbf{v}_I \times \mathbf{B}$, then an electromotive force $\omega_e \tau_e \mathbf{v}_I \times \mathbf{B}$ exists in the flow direction (Schluter 1951). Also, when the degree of ionization Ne/N_A is small compared to unity, there is an additional effect due to a relative velocity between the ions and neutral particles. For the special case outlined in the first paragraph of this Appendix, the velocity of the ions v_I in terms of the neutral particle velocity v_A is

$$v_I = \frac{v_A}{1 + \omega_I \tau_{IA} \omega_e \tau_e}, \tag{A 4}$$

where $\omega_I \tau_{IA}$ is the number of gyro orbits completed by the ions between collisions (Schluter 1951). Since $\mathbf{v}_A \times \mathbf{B}$ is the apparent electric driving force for currents, the effective conductivity in equation (11) will be reduced by the same factor as the electric field in the $(\mathbf{v}_A \times \mathbf{B})$-direction. Hence, $\sigma = \sigma_0/(1 + \omega_I \tau_I \omega_e \tau_e)$ which is equation (11). Finally, the current in the $(\mathbf{v}_A \times \mathbf{B})$-direction is

$$j_{\text{par}} = \left\{ \frac{\sigma_{\text{perp}}^2}{\sigma_{\text{par}}} + \sigma_{\text{par}} \right\} \left\{ \frac{v_A B}{1 + \omega_I \tau_{IA} \omega_e \tau_e} \right\}. \tag{A 5}$$

If σ_{perp} and σ_{par} are defined as in equations (A 2) and (A 3), the first factor in equation (A 5) equals σ_0.

Equations (A 2) and (A 3) were obtained from an analysis which neglects the variation of collision frequency with velocity. This analysis applies very well to the case where most of the collisions of the electrons are with neutral particles, and

the cross-section for momentum transfer does not change appreciably with the relative velocity between the particles.

For the experiments described in this paper, argon is sufficiently ionized so that electron-ion collisions are the governing factor. The electron-ion collision cross-sections are rapidly varying functions of velocity, and for these conditions the first factor on the right-hand side of equation (A 5) differs from σ_0. Landshoff (1949) has computed the transport properties of a completely ionized gas in the presence of a magnetic field to obtain σ_{par} and σ_{perp} as functions of $\omega_e \tau_e$. These values have been used to compute the theoretical gas current (dashed curve in figure 17).

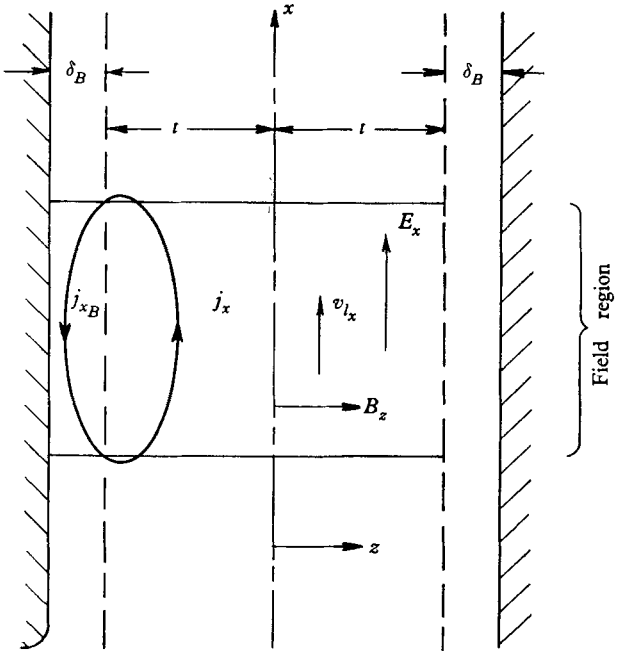

FIGURE 18. Schematic diagram of Region 4 (the y-direction is perpendicular to the plane of the drawing).

In order to estimate the importance of currents in the flow direction for the end geometry described in this paper, consider the following problem as illustrated in figure 18.

In a co-ordinate system where there is no motion of the ions in the x-direction, $E'_y = v_{Ix}B$. One may write the following expressions for the components of the current in the inviscid flow region

$$j_y = 2(\sigma_{\text{perp}} E_x + \sigma_{\text{par}} E'_y)t, \tag{A 6}$$

$$j_x = 2(\sigma_{\text{par}} E_x + \sigma_{\text{perp}} E'_y)t. \tag{A 7}$$

The boundary layer for this calculation is assumed to consist of a layer of gas of thickness δ_B with no motion relative to the wall. Hence, in this layer

$$E'_y = v_{Ix}B_Z = 0,$$

and the current in the x-direction becomes

$$j_{xB} = E_x \delta_B \sigma_{\text{par}_B} = \frac{E_x \delta_B \sigma_{0B}}{1 + w_{eB}^2}, \tag{A 8}$$

where $w_{eB} = \omega_e \tau_e$ in the boundary layer.

One may equate the currents in the x-direction in the inviscid region to the current in the boundary layer. This yields the expression

$$E_x = \frac{E_y' + \sigma_{\text{perp}}}{\sigma_{\text{par}} + \dfrac{\sigma_{0B} \delta_B}{1 + w_{eB}^2}}. \tag{A 9}$$

If this expression is substituted into equation (A 1) we obtain

$$j_y = \sigma_0 E_y' t \left\{ \frac{1 + \dfrac{\sigma_{0B}}{\sigma_0} \dfrac{\delta_B}{t} \left(\dfrac{1 + w_e^2}{1 + w_{eB}^2} \right) \left(\dfrac{1}{1 + w_{eB}^2} \right)}{1 + \dfrac{\sigma_{0B}}{\sigma_0} \dfrac{\delta_B}{t} \left(\dfrac{1 + w_e^2}{1 + w_{eB}^2} \right)} \right\}. \tag{A 10}$$

Since $E_y' = v_{Ix} B$, this yields the expression for j_y given in equation (13) of this paper.

REFERENCES

Landshoff, R. 1949 *Phys. Rev.* **76**, 904.

Lin, S. C., Resler, E. L. & Kantrowitz, A. R. 1955 *J. Appl. Phys.* **26**, 95.

Petschek, H. E. & Byron, S. 1957 *Ann. Phys.* **1**, 270.

Petschek, H. E., Rose, P. H., Kane, A., Glick, H. S. & Kantrowitz, A. R. 1955 *J. Appl. Phys.* **26**, 83.

Resler, E. L., Lin, S. C. & Kantrowitz, A. R. 1952 *J. Appl. Phys.* **23**, 1390.

Schluter, A. 1950 *Z. Naturf.* **5** A, 72.

Schluter, A. 1951 *Z. Naturf.* **6** A, 73.

Shapiro, A. H. & Hawthorne, W. R. 1947 *J. Appl. Mech.* **14**, 317.